Diffusion around a cardiac calcium channel and the role of surface bound calcium

Donald M. Bers* and Arthur Peskoff‡
*Division of Biomedical Sciences, University of California, Riverside, California 92521; and ‡Departments of Biomathematics and Physiology, University of California, Los Angeles, California 90024 USA

ABSTRACT The diffusion of Ca as it converges to the external mouth of a Ca channel is examined. Diffusional limitation on Ca ions entering Ca channels during current flow, cause local extracellular Ca depletions. Such extracellular Ca depletions have been reported in cardiac muscle. The cardiac sarcolemma has a large number of low-affinity Ca binding sites that can buffer these local Ca depletions. For a hemisphere of extracellular space (of radius < 0.33 μm) centered on the external mouth of a Ca channel the amount of Ca bound at the membrane surface exceeds that which is free within the associated hemisphere. The ratio of bound Ca/free Ca increases as r decreases, such that the [Ca] nearest the Ca channel is the most strongly buffered by sarcolemmal bound Ca. It is demonstrated that Ca ions coming from these sarcolemmal Ca binding sites contribute quantitatively to the integrated Ca current. The electric field generated by the local depletion of Ca near the channel mouth has little impact on the extent of Ca depletion, but if an additional electric field exists at the mouth of the channel, Ca depletion can be significantly altered. Other low-affinity Ca binding sites in the interstitium may also contribute to the buffering of extracellular Ca. The complex geometry of the extracellular space in cardiac muscle (e.g., transverse tubules and restrictions of extracellular space between cells) increases both the predicted Ca depletions (in the absence of binding) and the bound/free ratio. Thus, the impact of this surface Ca binding is greatly increased. By considering arrays of Ca channels in transverse tubules or in parallel planes (e.g., membranes of neighboring cells), extracellular Ca depletions are predicted which agree with those measured experimentally. Membrane Ca binding may also be expected to buffer increases in [Ca] around the inner mouth of Ca channels. It is demonstrated that in the absence of other intracellular systems most of the Ca entering the cell via Ca channels might be expected to be bound to the inner sarcolemmal surface. It is concluded that surface Ca binding may have a substantial impact on the processes of extracellular Ca depletion (and intracellular Ca accumulation).

INTRODUCTION

Striking correlations have been previously reported between the amount of Ca bound to the external surface of cardiac sarcolemma and contractility of cardiac muscle under a variety of conditions (Bers and Langer, 1979; Philipson et al., 1980*a*, *b*; Bers et al., 1981). It has been suggested that the amount of Ca bound at the sarcolemma is related to Ca influx and hence to tension development (whether directly or via induction of Ca release from the sarcoplasmic reticulum). Correlations have also been reported between tension development and the slow inward Ca current (I_{Ca}) (for example as a function of membrane potential during voltage clamp pulses, McDonald et al., 1975; London and Krueger, 1986). Furthermore, rapid depletions of extracellular Ca (Ca_o) occur with activation and correlations have also been demonstrated between tension development and these Ca depletions (Bers, 1983, 1985, 1987). A general goal of the present study is to begin to clarify the interrelationships between sarcolemmal Ca binding, extracellular Ca depletions, Ca current, and tension development.

These activation dependent extracellular Ca depletions have been demonstrated with both extracellular Ca microelectrodes (Bers, 1983, 1985, 1987; Dresdner and Kline, 1985; Shattock and Bers, 1989) and extracellular Ca sensitive dyes (Hilgemann, 1986; Cleeman et al., 1984) and are believed to represent Ca influx which is largely mediated by I_{Ca} (as these depletions are inhibited by Ca channel antagonists). The fact that such extracellular Ca depletions can be detected suggests that there is some diffusional limitation in the access of Ca ions to the Ca channel. The magnitude of the Ca depletion would also be expected to be greatest at the external mouth of the Ca channel. Under physiological conditions, the outer surface of the sarcolemma binds large quantities of Ca_o with low affinity. For example, at 2 mM Ca, the amount of Ca bound at these low-affinity sites far exceeds the Ca required to fully activate the cardiac myofilaments (Bers and Langer, 1979). Thus, when Ca enters the Ca channel, depleting the local [Ca], Ca will

Address correspondence to Donald M. Bers, Ph.D., Division of Biomedical Sciences, University of California, Riverside, CA 92521-0121.

dissociate from sarcolemmal sites nearby to limit the fall in local [Ca]. In this way, the sarcolemmal bound Ca could make a quantitatively large contribution to Ca which enters through Ca channels. These sarcolemmal Ca binding sites can serve as a substantial Ca buffer, although this aspect is not widely appreciated. A major aim of the present study is to calculate the quantitative changes in sarcolemmal bound Ca which may be expected to accompany Ca current flow. A second aim is to evaluate whether diffusional limitations on the access of Ca ions to Ca channels can be expected to be responsible for the Ca_o depletions observed in mammalian cardiac muscle (Bers, 1983, 1985, 1987; Hilgemann, 1986).

In the present study we examine the diffusion of Ca as it converges upon the mouth of a Ca channel. First we consider the Ca ions in a semiinfinite extracellular medium and the Ca ions bound to the planar membrane surface. As a result of geometric considerations for radii <325 nm, the number of ions bound to the surface is larger than the number of ions in a hemispheric volume centered on the channel mouth (especially for smaller values of r near the channel). The large number of bound Ca ions suggest an important Ca buffering role for these sites during local Ca depletions, which are predicted by application of the steady-state diffusion equation to this geometry. The contribution to the channel current from bound and free ions within a given radius are calculated. We also obtain the time-dependent solution to the diffusion equation for a step function channel current. We calculate depletions in the presence of binding and the contribution of bound and free Ca to the channel current as a function of time and space. For a 1 ms channel opening $\sim 50\%$ of the Ca ions passing through the channel are predicted to originate from sarcolemmal binding sites. Steady-state electrodiffusion equations are then applied and indicate that the simple diffusion results are valid when there is zero electric field at the channel mouth, but require some modification for nonzero fields. Some specific complications relevant to cardiac muscle are considered. For example, diffusion and depletion of Ca in the space between two neighboring cells is examined by considering arrays of Ca channels in two parallel planes. Ca diffusion and depletion in a transverse tubule is also examined by solving the diffusion equation inside a cylinder with conducting channels uniformly distributed along the length of the tubule. Consideration of these geometric constraints leads to predicted Ca_o depletions which match those measured experimentally. Finally, we apply the semiinfinite medium results to the intracellular mouth of the channel and estimate intracellular ion accumulation and changes in surface binding.

THEORY AND RESULTS

Ca binding to sarcolemma

Plasma membranes of many tissues exhibit low-affinity Ca binding. The passive Ca binding properties of cardiac muscle sarcolemma have been studied extensively and will be used as our model system (Bers and Langer, 1979; Philipson et al., 1980*a*, *b*; Bers et al., 1981, 1985, 1986). Under normal physiological ionic concentrations these low-affinity Ca binding sites are about half-saturated and in isolated sarcolemmal vesicles, Ca binding can reach ~ 300 nmol/mg of sarcolemmal protein. Assuming 1.2 μmol phospholipid/mg protein and 0.65 nm^2/2 phospholipid molecules (one on each side, or 2,300 cm^2/mg protein) this corresponds to $\sim 1.3 \times 10^{-18}$ mol/μm^2 or ~ 0.6 Ca binding site per nm^2. Typical Ca binding results are illustrated in Fig. 1 as a function of [Ca] in media similar to that expected extracellularly. We have previously developed a model to describe the Ca binding characteristics of these membranes using Gouy-Chapman theory with specific cation binding to phospholipid head groups (Bers et al., 1985). The negative surface charge concentrates cations at the membrane surface and the intrinsic association constant used for Ca was 7 M^{-1}. Whereas this model may be more realistic, for the present study the Ca binding will be assumed to be of the simple Michaelis-Menten type related to bulk concentration, that is:

$$\text{Bound Ca} = N/(1 + 1/K_a[\text{Ca}]), \qquad (1)$$

where N is the total number of binding sites and K_a is the apparent bulk association constant. The curve in Fig. 1 describes this relationship for $N = 320$ nmol/mg (or 1.38×10^{-18} mol/μm^2) and $K_{Ca} = 241$ M^{-1} where the

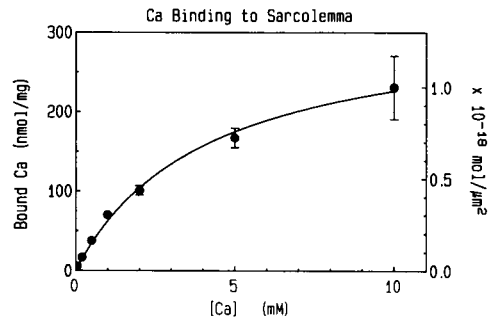

FIGURE 1 Ca binding to isolated rabbit cardiac sarcolemmal vesicles. The points (±SEM) are from Bers et al. (1985) and were measured in a medium containing 140 NaCl, 5 mM Hepes, and $CaCl_2$ as indicated at pH 7.4, 30°C. The curve is a least-square fit of this data on a Scatchard plot and is described by Eq. 1 where $N = 320$ nmol/mg and $K_{Ca} = 241$ M^{-1}.

higher K_a compensates for using bulk [Ca] in Eq. 1 rather than the higher surface [Ca] which results from the negative surface charge. This representation is sufficient for the present study and simplifies the calculations below. We do not include the Gouy-Chapman effects (Andersen, 1983; Hainsworth and Hladky, 1987) with the radial diffusion because this would dramatically complicate the mathematical treatment and may not make a large quantitative difference (see below).

Fig. 2 *A* shows a hemisphere of external solution around the mouth of a Ca channel. For the specific radius indicated, 30 nm and at 2 mM $CaCl_2$ + 140 mM NaCl, the number of Ca ions free in the hemisphere (68) and the number of Ca ions bound to the disk of membrane (764) are indicated. This radius is 150 times the assumed radius of the Ca channel (0.2 nm). Whereas McCleskey and Almers (1985) estimated the radius of a Ca channel to be ~0.27–0.3 nm, the difference does not affect the results in the present study. It can also be estimated that another 47 Ca ions would be in the screening or double layer compensating fixed negative charges (Bers et al., 1985). This figure indicates that within this radius most of the Ca ions (~92%) are bound to the surface membrane. The ratio of Ca bound/Ca free in such a hemisphere will depend upon radius (r), varying as $1/r$.

Fig. 2 *B* illustrates the radial dependence of bound and free Ca within such hemispheres and also indicates

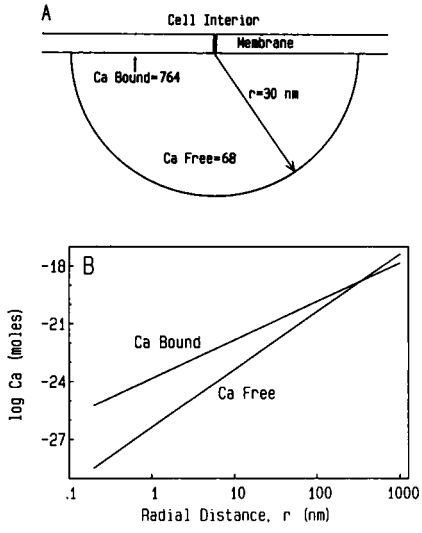

FIGURE 2 (*A*) Anticipated surface-bound Ca and free Ca (in number of ions) in a hemisphere of radius r = 30 nm from the external mouth of a Ca channel. (*B*) The number of Ca ions bound to the membrane or free in solution within hemispheres of radius r. The conditions for Ca binding are assumed to be as in Fig. 1 with [Ca] = 2 mM. The ratio of bound/free is 1,000 at 0.33 nm, 100 at 3.3 nm, 10 at 33 nm, and 1 at 325 nm.

how the bound/free ratio declines with increasing r. The point at which the bound and free Ca become equal is ~325 nm. It is of interest to note that Tsien et al. (1983), Bean et al. (1984), and McDonald et al. (1986) estimated the density of functional Ca channels in mammalian ventricular muscle to be ~4/μm². Thus, the crossover point in Fig. 2 *B* is in the range of overlap of neighboring Ca channel domains.

Steady-state diffusion in a semiinfinite medium

First we will consider a single Ca channel in a planar membrane in a semiinfinite medium with a constant Ca current, q. The solution of the diffusion equation describing the radial dependence of Ca concentration (as modified from Eq. 3.5b in Crank, 1975) is

$$c = c_o - \frac{q}{2\pi Dr}\left(erfc\left(\frac{r}{2\,(Dt)^{1/2}}\right)\right), \tag{2}$$

where c is the [Ca] at r and t, c_o is the bulk [Ca], D is the diffusion coefficient, and t is time. Eq. 2 is correct in the absence of binding. As t approaches ∞ (i.e., steady state), Eq. 2 reduces to $c = c_o - q/2\pi Dr$ and is valid even when binding is present. For the moment we will consider the steady-state case at long times where the complementary error function approaches one. The time dependence of Ca depletion is discussed below.

In the presence of a steady current, q, the number of free Ca ions within a hemisphere of radius r (Ca_F) will be

$$\begin{aligned} Ca_F &= \frac{2\pi}{3}c_o r^3 - \int_0^r \frac{q}{2\pi Dr'}\cdot 2\pi(r')^2\,dr' \\ &= \frac{2\pi}{3}c_o r^3 - \frac{q}{2D}r^2, \end{aligned} \tag{3}$$

where the right hand term is depletion of Ca ions due to current flow. If we further assume that in this steady state the Ca bound to the membrane at r has changed in accordance with the steady-state [Ca], then the number of Ca ions bound within the hemisphere of radius r, (Ca_B) is given by

$$\begin{aligned} Ca_B &= \int_x^r \frac{2\pi N r'\,dr'}{1 + \dfrac{1}{K_a\,(c_o - q/2\pi Dr')}} \\ &= 2\pi N\left\{\frac{(b-1)(r^2-x^2)}{2b} \right. \\ &\quad \left. - \frac{a(r-x)}{b^2} + \frac{a^2}{b^3}\ln\left(\frac{a-br}{a-bx}\right)\right\}, \end{aligned} \tag{4}$$

where $a = qK_a/2\pi D$ and $b = K_a c_o + 1$. The lower integration limit ($x = a/(b-1)$) coincides with the point

at which the predicted [Ca] becomes zero (i.e., $r = q/2\pi Dc_o$).

Fig. 3 shows the radial dependence of [Ca] assuming several different values of D and [Ca]. The aqueous diffusion coefficient for Ca has been estimated to be between 5.2×10^{-6} and 7×10^{-6} cm²/s (Wang, 1953; Hodgkin and Keynes, 1957; Kushmerick and Podolsky, 1969; Nasi and Tillotson, 1985). However, estimates of D for Ca in biological systems are considerably lower, e.g., $0.14–1.2 \times 10^{-6}$ cm²/s inside muscle and nerve cells (Hodgkin and Keynes, 1957; Kushmerick and Podolsky, 1969; Nasi and Tillotson, 1985) and $0.47–1.65 \times 10^{-6}$ cm²/s in muscle extracellular space (Niedergerke, 1957; Safford and Bassingthwaighte, 1977). Thus, we have chosen a range of values of D for Fig. 3.

The curves in Fig. 3 are illustrated for three different values of $[Ca]_o$ and I_{Ca}. Fig. 3 *A* indicates local [Ca] as a function of r for 2 mM bulk [Ca] with $I_{Ca} = 0.1$ pA for $D = 6$, 3, and 1×10^{-6} cm²/s. Fig. 3 *B* is for the same D values at lower [Ca] (0.2 mM) typical of that used in extracellular Ca depletion studies (e.g., Bers, 1983; Hilgemann, 1986) and assuming $I_{Ca} = 0.03$ pA. Single-channel Ca currents at 2 and 0.2 mM Ca were extrapolated from the concentration dependence of conductance of cardiac Ca channels by Yue and Marban (1990) assuming Ba conductance is ~3 times Ca conductance (see also Fenwick et al., 1982). For the same D values, Fig. 3 *C* assumes 100 mM Ca and 1 pA current, typical of patch clamp recording of single Ca channel currents with 100 mM Ba at a membrane potential of 0 mV or 100 mM Ca at ~ −30 mV.

The fractional depletion of Ca_o is smaller when bulk [Ca] is higher. This is an obvious consequence of the fact that the ratio C_o/q is higher at 100 mM Ca than 2 mM Ca (by fivefold). For the lower concentrations (Fig. 3, *A* and *B*) larger fractional depletions are predicted. Indeed, for $D = 1.0 \times 10^{-6}$ cm²/s and the assumed current, the local [Ca] falls to zero as r approaches the channel mouth and negative [Ca] is predicted. This, of course, is not physically possible, but it is not a serious limitation and could have multiple explanations. For example, the value of D (10^{-6} cm²/s) could be slightly too low, the value of q might be slightly high and local effects at very small values of r may lead to changes in [Ca] (such as local electric fields or "ion capture" by the channel). Local Ca depletion produced by a fixed I_{Ca} also produces a negative potential, which would draw more Ca ions into the region, lessening depletion. However, the influence of this electrodiffusive force in the absence of an external electric field is small compared to the depletion generated by the simple diffusion limitation. This electrodiffusion case will be described below (Eqs. 11 and 12).

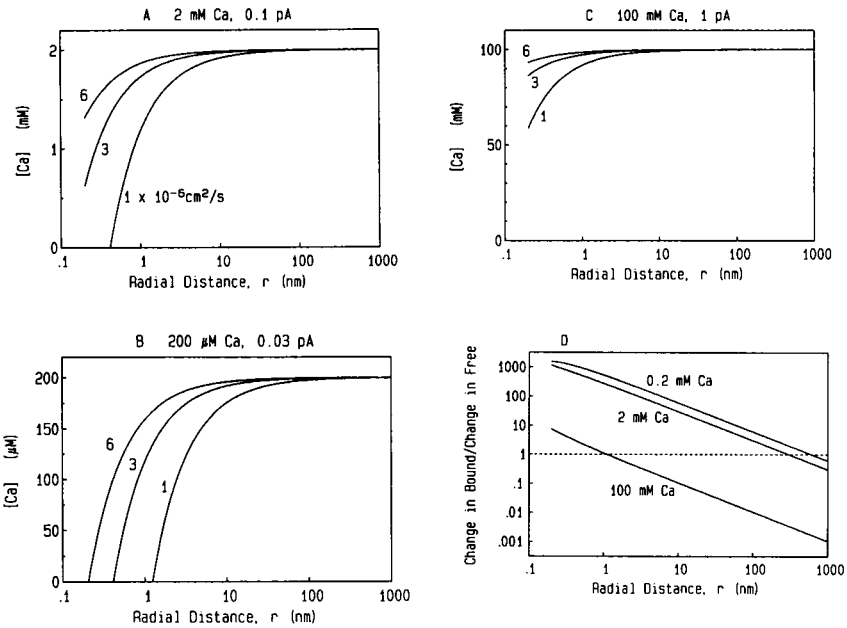

FIGURE 3 The radial dependence of steady-state [Ca] outside a Ca channel through which a constant current, q, is flowing. (*A*) Bulk [Ca] = 2 mM, $q = 0.1$ pA. (*B*) Bulk [Ca] = 200 μM, $q = 0.03$ pA. (*C*) Bulk [Ca] = 100 mM, $q = 1$ pA. The curves are calculated from Eq. 2 with the indicated values of D ($1–6 \times 10^{-6}$ cm²/s). (*D*) The ratios of changes in Ca bound/changes in Ca free during steady-state current flow, q, for the three cases in *A*, *B*, and *C* where $D = 6 \times 10^{-6}$ cm²/s. From top to bottom, $q = 0.03$, 0.1, 1 pA.

If we assume that the steady-state condition allows the sarcolemmal Ca binding sites to equilibrate with the local [Ca], the alteration in Ca binding can be estimated. Indeed the rate constants of adsorption and desorption of Ca at these low-affinity sites would be expected to be very fast (Eigen and DeMaeyer, 1963). Fig. 3 *D* shows how the ratio of the decrease in bound and free Ca changes as a function of r for the three cases in Fig. 3 (using Eqs. 3 and 4 with $D = 6 \times 10^{-6}$ cm^2/s). At 2 and 0.2 mM [Ca] the change in bound Ca is dominant whereas at 100 mM Ca the change in free Ca is dominant.

Time dependent diffusion in a semiinfinite medium

In the steady state, the calcium concentration is given by the $t = \infty$ limit of Eq. 2, $c = c_o - q/2\pi Dr$. This limit is correct even when there is Ca binding to the membrane surface because in the steady state there is no release of Ca and the ion flux is spherically symmetric, converging on the channel mouth. However, Eq. 2 is not valid during the transient period when Ca is being released from the binding sites. To study this transient period we must solve the diffusion equation subject to a boundary condition on the membrane surface that accounts for the flux of bound Ca into the bathing medium.

At $[Ca]_o < 2$ mM the binding shown in Fig. 1 can be approximated by a linear relation between the bound Ca concentration (moles/micron^2) and the bulk concentration (moles/micron^3), $Ca_B = kc$ (where $k = 0.2$ μm). This linearization greatly facilitates the mathematical analysis. These sites are also assumed to equilibrate instantaneously. If the kinetics of these sites were slower than (or comparable to) the timescale discussed below (usually milliseconds) then somewhat larger depletions would be expected.

We introduce cylindrical coordinates (r, z) with the origin $(0, 0)$ at the center of the channel mouth. The z-axis is along the channel axis where $z = 0$ is the membrane surface, and r is normal to the z-axis (parallel with the membrane surface). We assume cylindrical symmetry. Defining [Ca] as $c(r, z, t)$, the amount of Ca_B in moles/micron^2 at a distance r from the channel is

$$Ca_B(r, t) = kc(r, 0, t). \tag{5}$$

The time rate of change of Ca_B, the resulting flux J_{Ca} into the medium and the normal derivative of the bulk concentration at the membrane surface are related, using Fick's law of diffusion, by

$$J_{Ca} = -\frac{\partial}{\partial t} Ca_B(r, t) = -k \frac{\partial c}{\partial t}(r, 0, t) = -D \frac{\partial c}{\partial z}(r, 0, t), \tag{6}$$

where D is the diffusion coefficient for Ca.

If we assume that the channel begins to conduct an ion current of q mol/s starting at $t = 0$, the boundary/initial value problem for diffusion from the semiinfinite medium with linear binding on the membrane boundary is

$$D \nabla^2 c = \frac{\partial c}{\partial t}$$

$$D \frac{\partial c}{\partial z}(r, 0, t) = k \frac{\partial c}{\partial t}(r, 0, t) + \frac{q\delta(r)}{2\pi r},$$

$$c(r, z, 0) = c_o, \tag{7}$$

where $q\ \delta(r)/2\pi r$ is the flux density arising from ion channel current. The Dirac delta function, $\delta(r)$ signifies that the ion current, q arises only at a point at $r = 0$ and the scaling factor, $2\pi r$ is required for the surface integral to yield a total flux, q. For simplicity we have assumed that the current is switched on abruptly at $t = 0$ and remains constant at $t > 0$. Consequently we do not consider the dependence of current on electric potential or [Ca] on either side of the membrane. This would become important in cases where large depletions are predicted, where the current would be expected to decrease. To consider this would require modification of Eq. 7 to include a model of the channel.

The solution is an inverse Laplace transform of an infinite integral

$$c(r, z, t) = c_0 - \frac{q}{2\pi kD} \cdot \mathcal{L}^{-1}\left\{\frac{1}{s}\int_0^\infty J_0\left(\frac{r}{k}\zeta\right)\frac{\exp\left(-(\zeta^2 + s)^{1/2} z/k\right)}{(\zeta^2 + s)^{1/2} + s}\zeta d\zeta\right\}, \tag{8}$$

where s is the nondimensional Laplace transform variable and ζ is a dummy integration variable. See Appendix A for a derivation of Eq. 8 and the analytical methods used.

Fig. 4 *A* shows the radial dependence of $[Ca]_o$ along the membrane surface ($z = 0$) for several values of t for 2 mM bulk $[Ca]_o$, 0.1 pA and $D = 10^{-6}$ cm^2/s. For these small distances (from 1 to 10 times the channel radius) the time scale of concentration change is very rapid. Within ~10 μs the radial dependence is close to its steady-state value ($t = \infty$), which is the lowest curve and is the same as the lowest curve in Fig. 3 *A*. The dashed curve shows the radial dependence at $t = 0.4$ μs if no sarcolemmal Ca binding effects are considered (i.e., Eq. 2). In this case, the complementary error function is > 0.82 even at 0.4 μs, so the depletion is almost to the steady-state value ($t = \infty$). Comparison of the two curves for 0.4 μs (Fig. 4, with binding at top and without binding, dashed) emphasizes the effect that these sarcolemmal sites may have in limiting local Ca depletions.

Fig. 4 *B* shows the [Ca] at a longer time (40 μs) and longer distances from the channel along the membrane

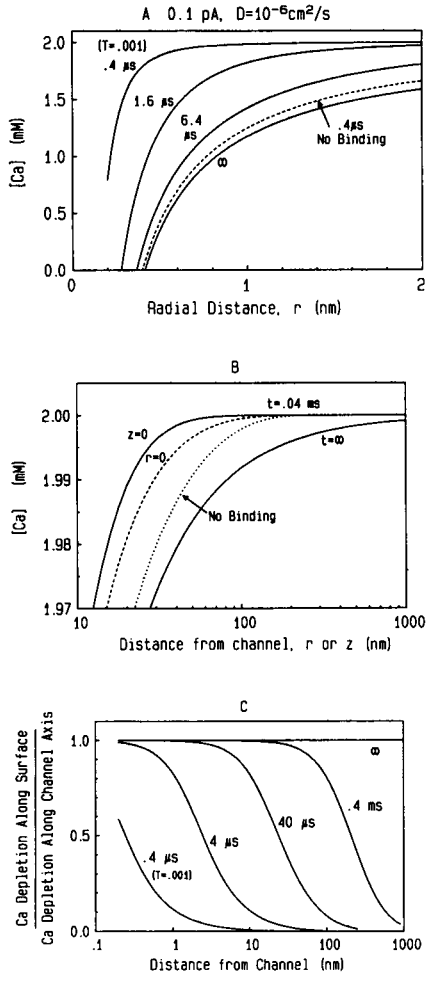

FIGURE 4 Time dependent changes of $[Ca]_o$ around a Ca channel. (*A*) Changes in $[Ca]_o$ at short times and distances, r from the channel. Nondimensional time $T = 0.001$ is equivalent to $t = 0.4$ μs (see below). The [Ca] approaches the steady-state curve (∞) which is the same as the bottom curve in Fig. 3*A* (i.e., $q = 0.1$ pA, $D = 10^{-6}$ cm²/s). The dashed curve is the predicted [Ca] at $t = 0.4$ μs in the absence of binding. (*B*) Comparison of changes in $[Ca]_o$ at $t = 0.04$ ms along the membrane surface ($z = 0$), along the axis of the channel ($r = 0$), when no sarcolemmal binding is considered (Eq. 2) and in the steady state ($t = \infty$). (*C*) Ratio of Ca_o depletion ($\Delta[Ca]_o$) along the membrane surface ($z = 0$)/Ca_o depletion along the channel axis ($r = 0$) for different values of t (0.4 μs-∞) for the same conditions as in *A*. Note that in the steady state ($t = \infty$) the r and z dependence of $[Ca]_o$ are the same. At all shorter times the depletion along the surface is smaller than along the channel axis. The curves are general solutions for Eq. 8 which can also be considered in nondimensional time, T (Dt/k^2), distance R (r/k) or Z (z/k) and depletion C ($(c - c_0)2\pi kD/q$) (see Appendix A, Eq. A2). For the dimensional example here $k = 0.2$ μm (see Eq. 5), $D = 10^{-6}$ cm²/s, $q = 0.1$ pA, and $c_0 = 2$ mM.

surface ($z = 0$), along the channel axis ($r = 0$), and in the absence of sarcolemmal Ca binding (where r and z are interchangeable). For these longer distances the longer time is appropriate, because this is the time scale over which depletion is occurring. For example, at 0.4 μs as used in Fig. 4*A*, virtually no depletion has occurred at $r = 10$ nm ($\Delta[Ca] = 4$ nM). Even at 40 μs the magnitudes of the Ca depletion in Fig. 4*B* are small, but we will see in Fig. 5 that the integrated contribution to the Ca current is substantial at these distances.

Fig. 4*B* demonstrates that depletion along the surface ($z = 0$) is smaller than along the channel axis ($r = 0$), which in turn is smaller than if there were no binding. This emphasizes the impact of binding on the Ca depletion, especially along the surface. At shorter times the curves are more widely separated. At longer times the curves get closer together and eventually converge to the steady-state solution ($t = \infty$). To illustrate this behavior over a wide range of times and distances, the ratio of the Ca depletion along the membrane surface to the Ca depletion along the channel axis is plotted in Fig. 4*C*.

The number of ions entering the channel that are attributable to the Ca that was bound to the surface and from the Ca in the hemisphere of radius r at $t = 0$, can be calculated by computing surface and volume integrals of Eq. 8. This is described in Appendix B (Eqs. B1 and B2). Fig. 5*A* shows the fraction of ions which constitute the Ca current from the hemispheric volumes of radius 0.05 μm to ∞ as a function of time. Fig. 5*B* shows the fraction

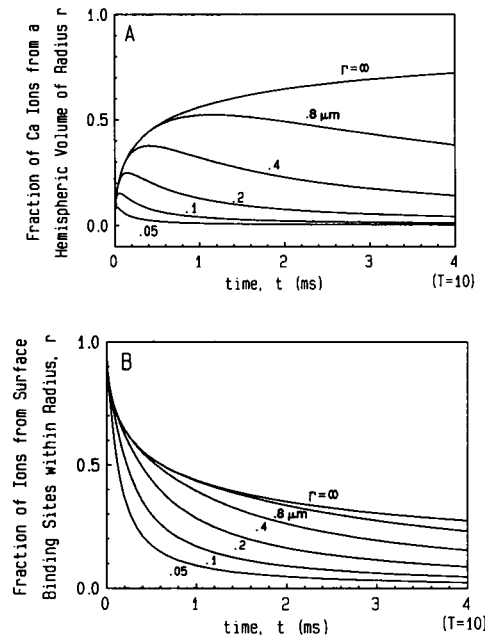

FIGURE 5 Time dependence of the change in Ca free and bound. This is the fraction of ions which constitute the current (qt), and come from the free solution within the hemispheric volume of radius r (*A*) or from sarcolemmal binding sites within radius r (*B*). The time is shown in both nondimensional units, $T = Dt/k^2$ and in milliseconds assuming $D = 10^{-6}$ cm²/s and $k = 0.2$ μm.

of ions making up the Ca current, which originated from within membrane circles of radius 0.05 μm to ∞ as a function of time. Note that the two $r = \infty$ curves in Fig. 5 add up to unity, indicating that the total change in bound and free Ca is exactly the same as the integrated current, qt. The curves show that there is a significant contribution to the total integrated current (qt) from Ca bound at distances up to 1 μm even though the depletions in Fig. 4 *B* are small in magnitude (e.g., note difference between 0.4 and 0.8 μm curves). This is a consequence of small depletions being multiplied by large volumes at large values of r. Certainly at times typical of single Ca channel open times (0.4–1.5 ms; Brum et al., 1984; Cachelin et al., 1983; Hess et al., 1984) a relatively large fraction of ions entering the cell (40–56%) would come from these surface sites.

Figure 6, *A* and *B*, show similar information, but as "snapshots" of the radial dependence for two values of t (0.4 and 1.6 ms). We see from Figs. 5 and 6 that at short times, bound Ca makes a relatively larger contribution to the current and most of that Ca originates from binding sites near the channel. For example, from Fig. 6 *A* we see that at $t = 0.4$ ms the Ca bound to the surface contributes more than half of the ions that have passed through the channel, and most of these ions originated from within a circle of radius 0.2 μm. At shorter times the relative contribution from the surface is larger and from a smaller circle, and for longer times the volume contribution dominates and the majority of the ions come from larger radial distances.

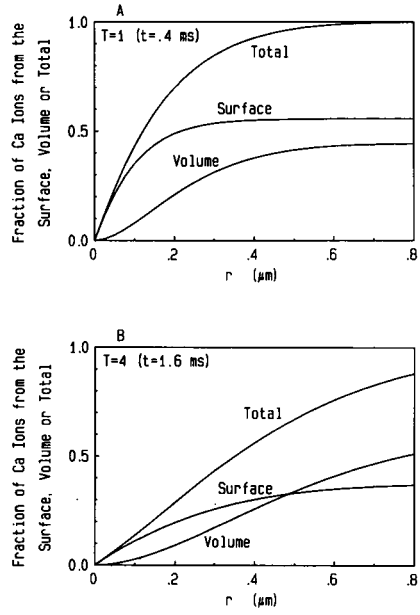

FIGURE 6 Changes in bound, free, and total Ca as function of r at two different times. This is the fraction of integrated Ca current (qt) which can be accounted for by decreases in the bound Ca (surface), free Ca (volume), and the sum of these (total) within a given radius, r. The curves are also general solutions where T is the nondimensional time, Dt/k^2 and R is the nondimensional distance, r/k (see Appendix A). For the present example k is assumed to be 0.2 μm (see Eq. 5) and D is 10^{-6} cm²/s. Note that for $D = 3$ or 6×10^{-6} cm²/s, $T = 4$ corresponds to 0.53 or 0.27 ms, respectively.

Steady-state electrodiffusion in a semiinfinite medium

So far we have analyzed the problem in terms of the simple diffusion equation. However, electrical forces should be included due to depletion of charge carrier (Ca) near the channel mouth and due to electric fields from the channel or fixed charges near the channel. Because of the complexity of the general problem that includes electrodiffusion, binding and time dependence, we limit our consideration to electrodiffusion in the steady state. The integro-differential equation for the steady-state electric potential around the mouth of a Ca channel carrying a current q in a Ca/Na/Cl electrolyte is a variation of the equation derived by Peskoff and Bers (1988, Eq. 7).

$$\frac{2\lambda^2}{r}\frac{d^2}{dr^2}(r\phi) = \exp(\phi) - (1 - 2\gamma)\exp(-\phi) - 2\gamma\exp(-2\phi) - 2\delta\exp(-2\phi)\int_r^\infty \exp(2\phi)\frac{dr'}{(r')^2}, \quad (9)$$

where $\delta = q/2\pi[\mathrm{Cl}]D$, $\gamma = [\mathrm{Ca}]/[\mathrm{Cl}]$, (in this instance [Cl] and [Ca] refer to bulk concentrations) ϕ is the nondimensional potential (FV/RT), and λ = Debye length. This is really a special case (for divalent cation current) of the general case of the linearized model described by Peskoff and Bers (1988, i.e., for $z_1 = 2, z_2 = -1, z_3 = 1$). Assuming $\phi \ll 1$ and a nondimensional current $2\delta/\lambda$ is small, Eq. 9 can be linearized as (see also Peskoff and Bers [1988])

$$\frac{\lambda^2}{r}\cdot\frac{d^2}{dr^2}(r\phi) = (1 + \gamma)\phi + \frac{\delta}{r}. \quad (10)$$

The solution in this case is

$$\phi = \frac{\delta/(1 + \gamma) - Sa}{(1 + (a/\lambda)(1 + \gamma)^{1/2})r}\cdot\exp[(1 + \gamma)^{1/2}(a - r)/\lambda] - \frac{\delta}{(1 + \gamma)r}, \quad (11)$$

where a is the radius of the channel mouth and $S = a(d\phi/dr)$ at a is the nondimensional inwardly directed

electric field at $r = a$ as described by Peskoff and Bers (1988). Using a linearized Boltzman distribution (i.e., $c = c_o \exp(-2\phi) = c_o(1 - 2\phi)$, Peskoff and Bers, 1988), the [Ca], c is

$$c = c_o - 2c_o\phi - q/2\pi Dr. \quad (12)$$

For the case of 2 mM $CaCl_2$ + 140 mM NaCl, $q = 0.1$ pA and $D = 6 \times 10^{-6}$ cm^2/s, with no electric field at $r = a$ (i.e., $S = 0$), the nondimensional current $2\delta/\lambda = 2.4 \times 10^{-3}$ and $\phi(a) = 9.5 \times 10^{-4}$ (or 2.4 μV). Thus, the linearization above appears to be justified. Indeed, the conditions for Ca current considered in the present study are within the range which Peskoff and Bers (1988) found that the exact solution for Eq. 9 was very well approximated by linearization (as in Eq. 10). Using Eq. 10 to calculate the [Ca] as a function of radius (with $S = 0$), the resulting curves were indistinguishable from those calculated from Eq. 2 in Fig. 3 (lowest curves in Fig. 7, *A* and *B*). This indicates that the depletion is principally due to simple diffusional limitation with electrodiffusion not playing a significant role under these conditions.

When there is an electric field (e.g., $S = 0.1$, which would correspond to the electric field at the mouth of the channel for transmembrane potential of ~100 mV; see Peskoff and Bers, 1988) $\phi(a) = -0.081$ (or 2 mV) for the same conditions as above. This more negative potential will increase [Ca] near the mouth of the Ca channel significantly. For the above case, the [Ca] at $r = a$ predicted from simple diffusion (Eq. 2), electrodiffusion (Eq. 12 with $S = 0$) and electrodiffusion with an additional electric field at $r = a$ (Eq. 12 with $S = 0.1$) are 1.313, 1.317, and 1.638 mM, respectively. This illustrates that a reasonable field can facilitate diffusion and limit the extent of extracellular Ca depletion. Fig. 7 shows the radial dependence of [Ca] predicted from Eqs. 11 and 12 for several values of S with $D = 6 \times 10^{-6}$ (Fig. 7*A*) or 10^{-6} cm^2/s (Fig. 7*B*). The largest S value (0.35) would approximate one electronic charge effectively at the center of the channel mouth (see Peskoff and Bers, 1988). It is notable that for the smaller value of D (Fig. 7*B*) the [Ca] profile is dominated by the diffusional limitation, such that the additional field considering electrodiffusion has little effect.

We can estimate the effect of electrodiffusion on bound and free Ca by combining Eqs. 11 and 12 with Eqs. 3 and 4

$$\Delta Ca_F = 2\pi c_o\left(\int_0^r (1 - 2\phi_o)(r')^2 dr' - \int_0^r \left(1 - 2\phi - \frac{q}{2\pi D c_o r'}\right)(r')^2 dr'\right), \quad (13)$$

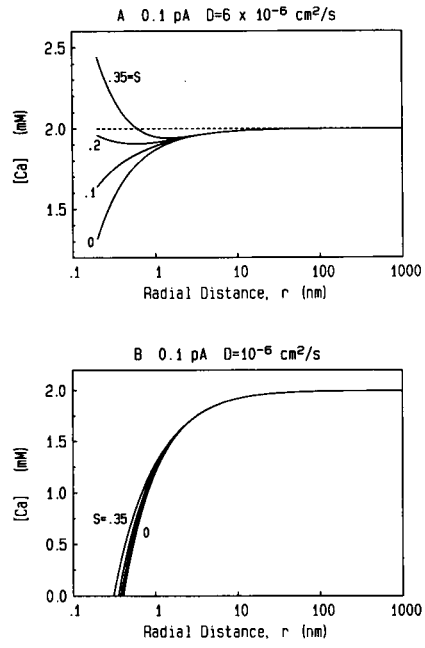

FIGURE 7 The radial dependence of steady-state [Ca] outside a Ca channel carrying a constant current, q. The curves were calculated using the linearized electrodiffusion model, Eqs. 11 and 12 with different values of nondimensional electric field, $S = 0$, 0.1, 0.2 and 0.35. Bulk [Ca] = 2 mM, $q = 0.1$ pA, and $D = 6 \times 10^{-6}$ cm^2/s in *A* and 10^{-6} cm^2/s in *B*. The $S = 0$ curves are indistinguishable from the simple diffusion case in Fig. 3*A*.

and

$$\Delta Ca_B = 2\pi N\left(\int_x^r \frac{r'dr'}{1 + \frac{1}{K_a(c_o - 2c_o\phi_o)}} - \int_x^r \frac{r'dr'}{1 + \frac{1}{K_a\left(c_o - 2c_o\phi - \frac{q}{2\pi Dr'}\right)}}\right). \quad (14)$$

where ϕ_o is the potential for zero current ($q = \delta = 0$). When the right side of Eq. 11 is substituted for ϕ, these expressions can be numerically integrated. Fig. 8 shows the calculated effect of electrodiffusion on the ratio of ΔCa bound/ΔCa free for 2 mM Ca (0.1 pA) and 100 mM Ca (1 pA). The curves for $\phi = 0$ are the same curves as in Fig. 3*D* (and are labeled $S = 0$, $\phi = 0$). The main effect of including electrodiffusion is a modest decrease of the ΔCa bound/ΔCa free ratio at small values of r (for $S = 0$ and 0.35) with a greater relative effect in the 100 mM Ca curves. This decrease is due to the nonlinear nature of the binding (i.e., bound/free decreases with increasing [Ca] as the sites become saturated).

This model does not include the dependence of [Ca]

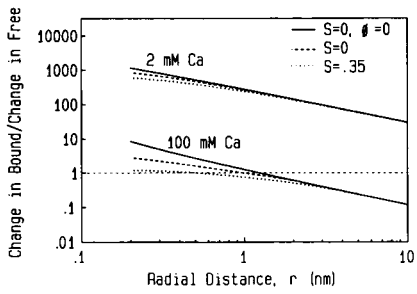

FIGURE 8 The ratios of changes in Ca bound/changes in Ca free during steady-state current flow, q (q = 0.1 pA for 2 mM Ca curves and q = 1 pA for 100 mM Ca curves). The solid curves, labeled $S = 0$, $\phi = 0$ are for the electroneutral case and are the same as the lower two curves in Fig. 3 D. $D = 6 \times 10^{-6}$ cm^2/s for all curves.

changes within the depth of the diffuse double layer where the [Ca] varies with distance from the membrane. However, an estimate of these changes can be made using the model of Ca binding and surface Ca of Bers et al. (1985). At 2 mM Ca, the amount of Ca in the double layer will be ~7.5% of that bound to surface sites (at 0.2 and 100 mM Ca these values would be 6.2 and 7.6%, respectively). When the [Ca] outside the double layer falls from 2 to 1 mM the amount of Ca in the double layer would fall by 40% whereas the Ca bound would fall by 35%. Looking at it another way, the decrease in double layer Ca would be only 8.4% of the change in bound Ca. Thus, the changes in double layer Ca are always small compared to the changes in bound Ca. The amount of double layer Ca will increase as r^2 (like bound Ca) rather than as r^3 (like free Ca) and will be quantitatively unimportant at both lower values of r where changes in bound Ca are dominant and at higher values of r where changes in free Ca are dominant. Consequently, our neglect of the [Ca] variation in the double layer will not significantly affect our results concerning relative changes in bound and free Ca.

The negative membrane surface charges will create a negative surface potential which influences the potential at the mouth of the Ca channel. This surface potential may be estimated to be about −37 mV for 2 mM $CaCl_2$ and 140 NaCl (using the model of Bers et al., 1985). This surface charge also increases surface [Ca] (to ~40 mM). However, if the Ca channel itself creates a small charge-free disk, the potential at the channel mouth will decline as a function of the radius of this disk (e-fold per λ). There is evidence that the skeletal muscle Ca channel is insulated from the bulk surface charge (Coronado and Holter, 1986). Arbitrarily assuming a charge-free disk of radius 3 nm (and using Eqs. 7 and 2 in Bers et al., 1985) $\phi(a)$ would only be 2% of the surface potential far from the disk (−0.9 mV) and [Ca] at $r = a$ would only be 7% greater than the bulk [Ca]. Thus, we expect the contribution of bulk surface charge to the electric field and [Ca] at the mouth of a Ca channel to be small. If there are intrinsic negative charges in the Ca channel protein itself, these could produce effects such as those described above for positive values of S (i.e., $S = 0.35$ would give a potential of −7 mV and a [Ca] increase of 56% at the channel mouth for $q = 0$).

Other factors in cardiac muscle

There are several other factors to be considered in cardiac muscle. These include: (*a*) overlapping Ca channel domains, (*b*) fixed negative charges in the extracellular space, and (*c*) geometric restrictions in the extracellular space.

If the density of functional Ca channels in cardiac muscle is assumed to be 3–5/μm^2 (Tsien et al., 1983; McDonald et al., 1986) then the distance between neighboring Ca channels would be ~400–600 nm. Thus, r = 200–300 nm would be halfway between neighboring Ca channels. Fig. 3 indicates that the amount of depletion is small for distances greater than 1–10 nm in the steady state, and Fig. 4 indicates even smaller distances for finite times. Thus, simultaneous openings of neighboring channels will have only a small effect on depletion close to a single channel. However, because of the long-range nature of the depletion (falling off as $1/r$ in the steady state from Eq. 2) the depletion will not approach zero far from the channel. In fact, if we naively sum an infinite number of uniformly spaced channels, the resulting depletion in the steady state would be infinite because the sum diverges. In the next section we will see that in the restricted space between two cells, where Ca channels are uniformly distributed over two parallel planes, the depletion increases linearly with time (which again is infinite at $t = \infty$, but micromolar in milliseconds). Because Ca channels inactivate, we restrict consideration to finite times which are physiologically relevant (see below).

The extracellular matrix in cardiac muscle bears fixed negative charge sites which may be expected to have at least weak Ca binding affinity. Cardiac muscle cells are also covered with a surface coat or "glycocalyx" which is rich in acidic sugars such as sialic acids (Langer et al., 1982). Along with intrinsic membrane glycoproteins the Ca buffering capacity of the extracellular space may be much larger than that due to the low-affinity sites of the membrane phospholipids. Some of these extracellular sites are distributed in the interstitial space and may well serve to buffer extracellular Ca depletions in a manner similar to that proposed here more specifically for the membrane sites. The distributed nature of these other sites would imply that the amount of Ca bound to them

would increase as r^3, thereby increasing the bound/free ratio throughout the interstitial space. This would provide additional buffering which could further limit extracellular Ca depletions. Despite this extracellular Ca buffering, extracellular Ca depletions *are* still observed (Bers, 1983, 1985, 1987). Unless the binding kinetics are too slow, more Ca must come off these other Ca binding sites during these extracellular depletions (which can last for many seconds). It seems unlikely that the off rates from these low-affinity sites would prevent them from functioning as effective extracellular Ca buffers. Thus, Ca from both membrane bound sites and interstitial sites may contribute quantitatively to Ca currents.

Another complicating factor in these considerations is the complex geometry of the extracellular space. The semiinfinite model described above may be relevant for a surface Ca channel in an isolated cell in a large bath. However, Ca channels in intact tissues would be subject to restrictions in the extracellular space (such as transverse tubules, intercellular clefts and neighboring cells) as well as the additional Ca buffering described above. Below we will consider two idealizations of these geometries. First we assume that the Ca channels are distributed over the surfaces of two parallel infinite planes, representing the membranes of two adjacent cells (see Fig. 9*A*). In mammalian cardiac muscle the distance between cells is typically 0.1–0.2 μm. Within this distance the ratio of Ca ions bound to the sarcolemma/Ca ions free in the space between the planes is about one or two (for 2 mM Ca) such that half to two-thirds of the total extracellular Ca would be sarcolemmal bound. In this case there is less free Ca (i.e., because the maximum radial distance is restricted by the neighboring cell) so that larger Ca_o depletions are expected and the relative contribution of bound Ca to current flow should be higher (due to a lower limit on the bound/free ratio). The ratio of bound/free Ca in a transverse tubule would be even greater (i.e., about four for a transverse tubule of radius 0.1 μm). Furthermore, if as in skeletal muscle, Ca channels are preferentially concentrated in transverse tubules (Almers et al., 1981), the Ca depletions there and the importance of the bound Ca as a source of Ca buffering would be even greater. These bound/free ratios do not include any Ca binding sites in the extracellular matrix. Inclusion of these would make these ratios even higher.

We can also use this sort of parallel plane model to consider depletion in the overall extracellular space (which includes capillaries, etc.). The surface/volume ratio (0.33 $\mu m^2/\mu m^3$) and fraction of extracellular space (25–30%) in ventricular muscle imply that there is ~1 μm^3 of extracellular space per micron^2 of sarcolemma (Page, 1978; Frank and Langer, 1974). Thus, we could lump the entire extracellular space as the space between two planes which are 2 μm apart (which may serve as an upper limit). These two cases of Ca channels in planes 100–200 nm apart and 1–2 μm apart are considered in the next section.

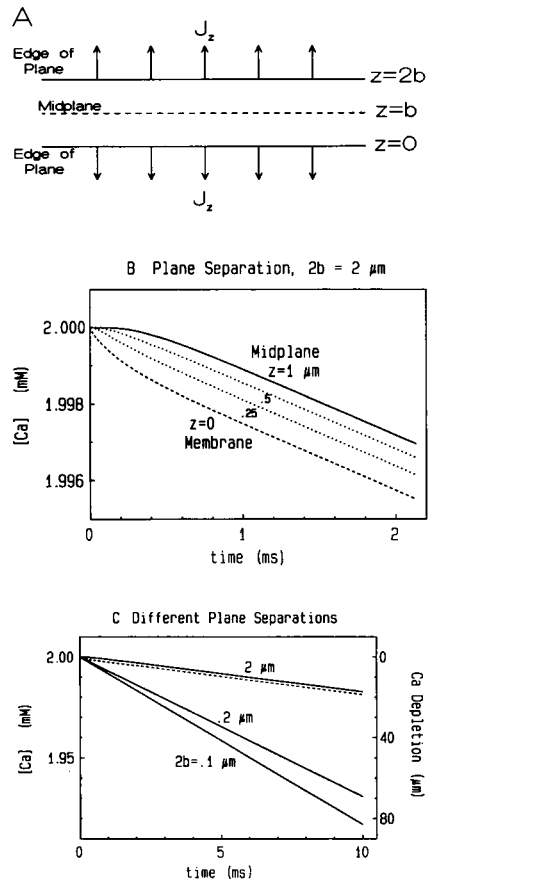

FIGURE 9 Ca depletion between two parallel planes containing Ca channels. (*A*) An edge view of the parallel planes. Ca depletion as a function of time at the midplane (*solid curves*) and at the membrane surface (*dashed curves*) for *B*, the upper limit of separation of planes ($2b$ = 2 μm), and *C* two lower values (0.1 and 0.2 μm). The deviation between the membrane and midplane curve is lower for smaller values of b. In *B* two intermediate curves are shown for 25 and 50% of the way from the membrane to the midplane (z = 0.25 and 0.5). Curves were calculated for 2 mM Ca_o, 0.1 pA, 4 channels/μm^2, k = 0.2 μm and D = 6×10^{-6} cm^2/s.

Diffusion between two parallel planes

To consider Ca depletion between two parallel planes we could, in principle, superimpose our single-channel solution for many channels distributed on the surface of two parallel planes. But because of the long-range nature of the depletion (i.e., in the steady state it drops off as $1/r$ for large r) the major contribution comes from

the summation of distant channels and for these it is sufficient to model the ion current as a uniformly distributed flux density over the two parallel planar surfaces.

The justification for this is that the average depletion so calculated will be much larger than the depletion calculated above for a single channel at distances comparable to the intercellular spacing or at distances comparable to the distance between two conducting channels. On the other hand, it will be much less than the single channel result close to the channel, so the above results are valid close to a channel.

For the case illustrated in Fig. 9*A*, of a uniform flux density of magnitude J_z normal to each of two parallel planes located at $z = 0$ and $z = 2b$, directed outward from the enclosed volume (slab), the boundary/initial-value problem is, for $0 \le z \le b$,

$$D\frac{\partial^2 c}{\partial z^2} = \frac{\partial c}{\partial t}$$

$$D\frac{\partial c}{\partial z}(0,t) = k\frac{\partial c}{\partial t}(0,t) + J_z$$

$$\frac{\partial c}{\partial z}(b,t) = 0$$

$$c(z,0) = c_o. \qquad (15)$$

We have used the symmetry of the problem about the midplane $z = b$ to obtain the boundary condition at $z = b$, which states that no flux crosses the midplane.

The solution to this problem is obtained in Appendix C, using the Laplace transformation technique. The result is

$$c(z,t) = c_o\frac{kJ_z}{D} \cdot \mathcal{L}^{-1}\left\{\frac{1}{s}\cdot\frac{\cosh(s^{1/2}(b-z)/k)}{s^{1/2}\sinh(s^{1/2}b/k) + s\cosh(s^{1/2}b/k)}\right\}, \qquad (16)$$

where, as before, s is a nondimensional Laplace transform variable. For $t \gg k^2/D$ (or 67 μs for $D = 6 \times 10^{-6}$ cm²/s), Eq. 16 can be approximated by

$$c(z,t) \sim c_o - \frac{J_z}{k+b}\left[t + \frac{1}{2D}\left((b-z)^2 - \frac{b^2(3k+b)}{3(k+b)}\right)\right]. \qquad (17)$$

Eq. 17 is obtained from Eq. 16 as described in Appendix C. It may also be obtained directly from Eq. 15.

The term linear in t in Eq. 17 ($-Jt/(k+b)$) in fact can be found by simply dividing the number of ions which leave the extracellular space in time t by the volume of the space. The depletion is less than Jt/b because of the contribution of bound Ca.

Fig. 9*B* is for an intercellular spacing ($2b$) of 2 μm which corresponds to the upper limit obtained by lumping the entire extracellular space to the volume between the planes (see above). The density of Ca channels is assumed to be 4/μm² and for 0.1 pA current per channel, $J_z = 2 \times 10^{-18}$ mol/μm²/s. The depletion at the membrane precedes that at the midplane, but after ~1 ms both curves become linear and parallel, separated by ~1.5 μM. The slope of these lines is −1.7 μM/ms (i.e., $-J_z/(k+b)$) such that it would take ~23 ms to reach the 40 μM depletion which is measured experimentally under these conditions (Bers, 1983). The narrower spacings in Fig. 9*C* ($2b$ = 0.1 and 0.2 μm) corresponds to the typical space between neighboring cells. The [Ca] gradient from membrane to midplane is smaller and the rate of depletion is faster such that 40 μM Ca_o depletion is reached in 4–6 ms. The first 10–20 ms is also the time during which the largest fraction of integrated Ca current is measured experimentally. Thus, the "square wave" of current used in the model is most reasonable for these short times. Given the slow response time of the Ca electrodes used to measure these depletions and complications due to temporally overlapping Ca efflux (via Na/Ca exchange, Bers, 1987; Hilgemann, 1986; Shattock and Bers, 1989) the agreement with these theoretical predictions is reasonably good.

Diffusion in a cylindrical tubule

We shall consider further the cylindrical case representing the interior of a transverse tubule of radius a, where there is a specified density of Ca channels producing a constant radial flux of Ca ions out of the tubule (and into the cell, see Fig. 10*A*). Let J_x denote the axial flux density (flux per unit cross-sectional area inside the tubule), J_a the radial flux density (flux per unit surface area) leaving the tubule through Ca channels and Ca_B the surface density of Ca ions bound to the membrane. Then the conservation of ions from the disc between x and $x + dx$ requires that

$$[J_x(x+dx,t) - J_x(x,t)]\,\pi a^2 + \left[J_a + \frac{\partial Ca_B}{\partial t}\right]2\pi a\,dx = -\frac{\partial c}{\partial t}\cdot\pi a^2 dx. \qquad (18)$$

Dividing by $\pi a^2\,dx$ and letting $dx \to 0$

$$\frac{\partial J_x}{\partial x} + \frac{2}{a}\left(J_a + \frac{\partial Ca_B}{\partial t}\right) = -\frac{\partial c}{\partial t}. \qquad (19)$$

Let $Q = 2J_a/a$ be the flux density per unit length leaving through the membrane and as in Eq. 5 assume that the binding can be approximated by a linear function of the concentration, $Ca_B = kc$. Using the relation $J_x = -D$

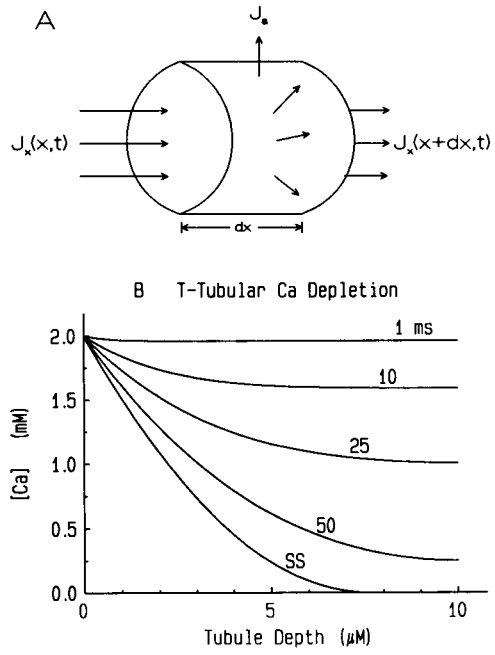

FIGURE 10 Ca depletion in a transverse tubule. (*A*) A cross-section of the cylindrical or transverse tubular model. Longitudinal flux density along the length or x-axis of the tubule is J_x and transmembrane flux density through Ca channels in the tubule wall of the tubule of radius a is J_a. (*B*) Ca concentration as a function of depth, x within a transverse tubule of radius a = 0.1 μm and length ℓ = 10 μm. The upper five curves are calculated from Eq. 22 for the indicated times after the start of a constant current flow (0.1 pA through each Ca channel, 4 channels/μm² of tubular wall, Q = 41.4 mM/s). The steady-state curve ($t = \infty$) is calculated from Eq. 23. These curves are for $D = 6 \times 10^{-6}$ cm²/s. The times (in milliseconds) are for no binding and should be multiplied by five for inclusion of the effect of bound Ca.

$\partial c/\partial x$ to eliminate J_x, Eq. 19 becomes

$$D\frac{\partial^2 c}{\partial x^2} - \left(1 + \frac{2k}{a}\right)\frac{\partial c}{\partial t} = Q. \tag{20}$$

This is the one-dimensional diffusion equation taking into account the contribution of the bound ions and the flux through the membrane. Defining a new time variable $t' = t/(1 + 2k/a)$ Eq. 20 may be written

$$D\frac{\partial^2 c}{\partial x^2} - \frac{\partial c}{\partial t'} = Q, \tag{21}$$

which is the usual diffusion equation with t replaced by t'. Thus the effect of the bound ions is simply to stretch the time dependence of the concentration by a factor of $1 + 2\,k/a$ (which for a 0.1 μm radius transverse tubule would be 5.0). For the remainder of this section we will use Eq. 21 with t (i.e., without binding) rather than t' (with binding).

If the tubule is open at $x = 0$ to a medium in which the concentration is a constant value c_o, the boundary condition at $x = 0$ is $c(0, t) = c_o$. If the tubule is closed at $x = \ell$ the boundary condition at $x = \ell$ is $\partial c/\partial x\,(\ell, t) = 0$. Assuming that the channels are nonconducting before $t = 0$ and the interior of the tubule is equilibrated with the bulk solution, $c(x, 0) = c_o$. The diffusion equation (Eq. 21), subject to these boundary and initial conditions may be solved. The solution is a quadratic function of x plus a Fourier sine series (see Appendix D).

$$c(x,t) = c_o - \frac{Qx}{D}\left(\ell - \frac{x}{2}\right) + \frac{2\ell^2 Q}{\pi^3 D}\sum_{n=0}^{\infty}\frac{\sin\left[\left(n+\frac{1}{2}\right)\frac{\pi x}{\ell}\right]}{\left(n+\frac{1}{2}\right)^3} \cdot \exp\left(-\left(n+\frac{1}{2}\right)^2 \pi Dt/\ell^2\right). \tag{22}$$

The concentration $c(x, t)$ in Eq. 22 has been computed and is illustrated in Fig. 10 *B* for a transverse tubule of radius 0.1 μm and depth (ℓ) 10 μm. For long times ($t \gg \ell^2/\pi^2 D$), the Fourier sine series is negligible and the solution relaxes to the first two terms. However, Eq. 22 is valid only for values of t and Q/D where it predicts $c > 0$ for all values of x. If Eq. 22 predicts $c = 0$ for any value of $x < \ell$ then a different boundary condition applies where c goes to zero (see Appendix D). In particular, the steady-state solution ($t = \infty$) for such cases is not given by the first two terms of Eq. 22, but rather by (from Appendix D)

$$c(x,\infty) = \begin{cases} c_o\,[1 - (Q/2Dc_o)^{1/2}\,x]^2, \text{ for } 0 \le x \le (2Dc_o/Q)^{1/2} \\ 0, \text{ for } (2Dc_o/Q)^{1/2} \le x \le \ell. \end{cases} \tag{23}$$

The results in Fig. 10 *B* illustrate that much larger Ca depletions would be expected in the transverse tubules than at the cell surface. Furthermore, the higher bound/free ratio of four in the transverse tubules implies that the decrease in bound Ca at steady state would be four times as large as the decrease in free [Ca]. This also means that ~80% of the Ca going through the channels from the transverse tubule will have originated from sarcolemmal sites. The steady state, however, will also take five times longer to reach.

To consider the region near an individual channel in the transverse tubule the semiinfinite solution can be combined with the tubule model as follows. A single channel in the tubule is essentially like the semiinfinite case except that the bulk [Ca] is given by the transverse tubule model (and Δ bound/Δ free has a lower limit of four). This is valid because the distances between channels (and the radius of the tubule) is large compared to the region where depletion is large (see Fig. 3).

Inner mouth of a Ca channel

We can also examine what may be expected at the inner mouth of a Ca channel. Fig. 11 *A* illustrates the $[Ca]_i$ profiles anticipated for $q = 0.1$ pA, resting $[Ca]_i = 100$ nM and various values for D. The [Ca] near the channel reaches millimolar levels and the [Ca] is substantially elevated with respect to the 100 nM baseline for a considerable radial distance. Even at $r = 1$ μm, $[Ca]_i$ is elevated to 237–1,470 nM in this example.

The inner sarcolemmal surface may also serve to buffer the rise in free [Ca] around the inner mouth of a Ca channel. There is no reason to expect fewer Ca binding sites on the inner surface of membrane phospholipids. Indeed, membrane phospholipids are distributed asymetrically with more acidic moieties on the inside (e.g., Zwall et al., 1973; Post et al., 1988) such that there may be more low-affinity Ca-binding sites inside. At physiological $[Ca]_i$ with the Ca binding measured experimentally (Bers et al., 1986) the ratio of changes in sarcolemmal bound Ca/free Ca at given r can be estimated (as in Fig. 3 *B*). The resting bound/free ratio is much higher than for the extracellular case and exceeds one even at $r = 10$ μm (about the radius of a cardiac muscle cell).

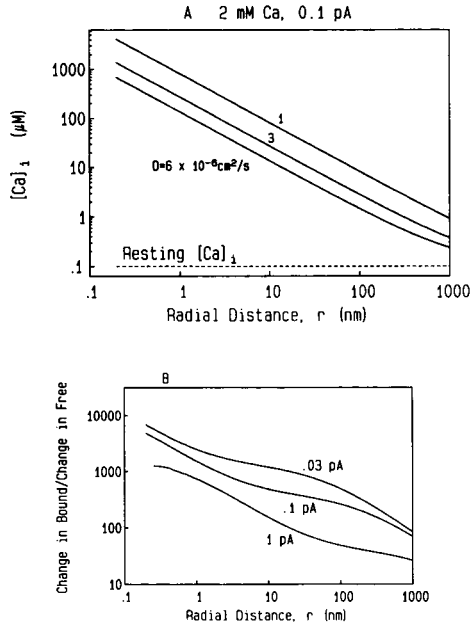

FIGURE 11 Ca accumulation at the inner mouth of a Ca channel. (*A*) Radial dependence of steady-state [Ca] around the inner mouth of a Ca channel with a constant current ($q = 0.1$ pA). Curves were calculated using Eq. 2 with $[Ca]_i = 10^{-7}$ M and $D = 1, 3$, and 6×10^{-6} cm²/s. (*B*) The ratios of changes in Ca bound/changes in Ca free around the inner mouth of a Ca channel during steady-state current flow ($q = 0.03, 0.1$, and 1 pA and $D = 6 \times 10^{-6}$ cm²/s). The curves were calculated from Eqs. 3 and 4 with an additional integral for a second small class ($N' = 3 \times 10^{-20}$ mol/μm², or 7 nmol/mg protein) of high-affinity sites ($K'_a = 10^6$ M^{-1}). Resting $[Ca]_i$ was assumed to be 0.1 μM. At this $[Ca]_i$, the resting Ca bound/Ca free ratio falls from 2×10^5 at $r = 0.2$ nm to 40 at $r = 1$ μm.

With current flow (0.10 pA) the ratio of changes in bound/free predicted by Eqs. 3 and 4 are shown in Fig. 11 *B*. In this case the single class of low-affinity Ca binding sites is inadequate to describe Ca binding at both high [Ca] (near the channel) and low [Ca] (further away from the channel). Therefore, we have used an additional small class of high-affinity Ca binding sites ($N' = 3 \times 10^{-20}$ mol/μm², or 7 nmol/mg, $K'_a = 10^6$ M^{-1}) which agrees with experimental measurements at micromolar levels of Ca (Bers et al., 1986). The results in Fig. 11 *B*, suggest that most of the Ca entering the cell would end up bound to the plasma membrane. This is obviously an oversimplification because numerous intracellular sites participate in Ca binding and transport. However, these considerations emphasize that the low-affinity sarcolemmal binding sites may constitute a very large potential Ca locus. That is, these sites may be capable of binding up to ~1 mmol Ca/kg wet weight of heart (Bers and Langer, 1979). Even under normal intracellular conditions, the inner sarcolemmal surface may bind ~30 μmol Ca/kg wet weight (Bers et al., 1986). When local [Ca] rises (as in Fig. 11) in the vicinity of a Ca channel, these sites might serve to damp these $[Ca]_i$ changes. Whether these low-affinity sites effectively buffer [Ca] changes due to Ca current flow would depend to a large extent on the binding kinetics (which are unknown). There are certainly other intracellular Ca buffers and diffusional restrictions which may also slow diffusion from the surface (Fischmeister and Horackova, 1983).

These intracellular [Ca] changes are obviously of importance in processes which are regulated by Ca influx (e.g., cardiac muscle excitation-contraction coupling). However, critical information about diffusional restrictions in these regions and the precise location where Ca participates in regulation is still required to extend the present consideration to such processes.

DISCUSSION

Relation to reported Ca_o depletions

Extracellular Ca depletions occur in cardiac muscle under physiological conditions (Bers, 1983, 1985, 1987; Dresdner and Kline, 1985; Hilgemann, 1986). This suggests that there may be diffusional limitation of Ca ions to the mouth of Ca channels. The present study indicates that local Ca_o depletions are expected on theoretical grounds. Maximum Ca_o depletions at individual excitations in mammalian cardiac muscle have been

reported to be ~8 μM in 0.2 mM bulk Ca and ~40 μM in 2 mM bulk Ca (Bers, 1983, 1985, 1987; Hilgemann, 1986). For the conditions and D values illustrated in Fig. 3 for a single channel in a semiinfinite region, this would correspond to the [Ca] at r = 5–30 nm and 3–20 nm for bulk [Ca] = 0.2 and 2 mM, respectively. Although it is not known how close to the cell membrane the Ca-selective microelectrodes are in the studies by Bers, it seems likely that the extracellular dye signals reported by Hilgemann (1986) are fairly representative of the changes in mean $[Ca]_o$. For the semiinfinite hemisphere to adequately explain these depletion magnitudes, the distance of the average place in the extracellular space from a Ca channel in mammalian heart muscle would have to be on the order of 10–20 nm. Such values are probably too small indicating that other factors affecting the extent of Ca_o depletion must be considered.

Two major complicating factors in cardiac tissue which will increase the magnitude of Ca_o depletions are diffusional barriers due to tissue geometry and overlapping Ca channel domains. For the cases of the parallel planes and transverse tubule (Figs. 9 and 10), the depletions of Ca_o are expected to be much greater than for the analogous semiinfinite hemisphere (at distances > ~10 nm from an individual channel, Fig. 3 *A*). Furthermore, if one considers that up to ~3.7% of the extracellular space in mammalian cardiac muscle may be inside transverse tubules (Page et al., 1971; Frank and Langer, 1974) it is possible that the Ca_o depletion signals recorded with Ca-sensitive dyes (Hilgemann, 1986) are dominated by a much larger transverse tubular depletion. For example, if the general extracellular depletion was only ~1 μM (Eq. 3, Fig. 3 *A*, $D = 6 \times 10^{-6}$, r = 200 nm) and mean transverse tubular depletion was ~400 μM (e.g., Fig. 10, 10 ms curve) the observed depletion would be ~20 μM (assuming a linear signal). However, the dye experiments of Hilgemann (1986) were performed in rabbit atrium which may have only sparse transverse tubules (Sommer and Jennings, 1986). This explanation would also not be tenable for the extracellular Ca microelectrode results because the electrode tip (4–15 μm diameter) cannot be in a transverse tubule (Bers, 1983, 1985, 1987). The quantitative similarity with these two different experimental approaches might mean that they really are both recording essentially mean extracellular [Ca].

The actual timecourse of Ca_o depletions recorded at individual contractions with extracellular Ca microelectrodes is variable, but typically reaches its maximum in ~50 ms (Bers, 1987). The rate of recorded depletion was reported to vary more than the extent of maximum depletion. This result could be explained by a variability in the shape of the extracellular region where the electrode tip resides. If this is true, it would tend to support the proposition that the mean extracellular Ca depletions are being measured with both techniques, but how close the Ca-electrode tip is to the site of maximum depletion will influence the observed timecourse. Measured extracellular Ca depletions are also complicated by temporally overlapping Ca efflux (e.g., via Na/Ca exchange) unless the conditions are such that Ca efflux is minimized (Bers, 1987; Hilgemann, 1986).

There is reasonable agreement between the Ca_o depletions predicted by the parallel plane model (Fig. 9) and the experimentally measured depletions. We can also extend our consideration of the transverse tubule geometry to include the reduction of [Ca] resulting from convergence to the surface opening of the tubule. This is really a special case of the radial diffusion problem with the tubular opening replacing the single channel and the total tubular current replacing the single channel current. At a radial distance of 1 μm the Ca_o depletion predicted by Eq. 2 (for $t = \infty$) is 4–20 μM and at 200 nm the Ca_o depletion is 17–100 μM (for $D = 6$ and 1×10^{-6} cm^2/s with bulk [Ca] = 2 mM, 0.1 pA/channel and 25.1 channels/tubule). Thus, the earlier assumption about constant [Ca] at the mouth of the transverse tubule is not strictly valid, but is satisfactory because [Ca] only decreases by 1–5%. It would also take 58 or 350 ms for the depletion 1 μm away from the T-tubule to reach 90% of this steady-state level (for $D = 6$ and 1×10^{-6} cm^2/s, respectively). This agrees with the timecourse and amplitude of Ca_o depletions predicted in the parallel plane model and measured experimentally (Bers, 1987). This is obviously a simplified consideration, but makes the point that a substantial depletion in the nontubular extracellular space may be due to tubular Ca current flow. Thus, regardless of whether the Ca channels are mainly in transverse tubules, on the sarcolemmal surface or evenly distributed, the projected Ca_o depletions are in the range observed experimentally.

Extracellular Ca binding sites and Ca_o depletions

The large number of Ca binding sites in the extracellular space would tend to reduce the magnitude of Ca_o depletions. These binding sites effectively prolong the time required to reach a steady state. This is clearly illustrated for sarcolemmal sites in the hemispherical case in Fig. 4 and for the cylindrical (or transverse tubular) case where the effect of sarcolemmal binding is primarily to increase the time by a factor of five. With the addition of other Ca binding sites in the extracellular space, the depletion profiles would be slower still. This leads to the conclusion that, particularly at short times,

local Ca depletion will be buffered by low-affinity Ca binding sites. Furthermore, this implies that a substantial fraction of the Ca supporting I_{Ca} at relatively short, physiologically relevant times would be expected to come from Ca binding sites (see Fig. 6). For example, in transverse tubules this would be >80%, by an amount which would depend on the number of binding sites in the glycocalyx which fills the tubules (Frank and Langer, 1974). Nearly half of the sarcolemma in rabbit ventricular myocytes is in transverse tubules (Page, 1978) and if the density of Ca channels is higher in the tubules (as in skeletal muscle, Almers et al., 1981) most of the Ca channels could also be in the tubules.

We can also estimate how large an extracellular Ca_o depletion might be expected based on purely experimental measurements of I_{Ca} and the size of the extracellular space. For a 2 nA peak I_{Ca} in a 14 μm diameter, 100 μm long myocyte, and again assuming 25% of the intact tissue is extracellular space, the depletion would be 2 μM/ms at peak I_{Ca}. This is similar to the linear rate of Ca_o depletion predicted in the parallel plane model (Fig. 9 *B*) where the Ca current is modeled as a square wave with a "lumped" extracellular space between the planes. The integrated Ca current measured in this cell over a 200 ms voltage clamp pulse is 0.4×10^{-15} mol (Bers, D. M., unpublished observation). This would correspond to a 82 μM depletion of the extracellular space and is about twice the size of the observed Ca_o depletions at 2 mM Ca_o (Bers, 1983). These experimental results are expected if some of the Ca which enters the cells comes from extracellular binding sites. Thus, the measured decline in free $[Ca]_o$ is less than that transported by the Ca channels as predicted by the models described in the present study.

Timecourse of Ca current

On the basis of the foregoing, one might suppose that single-channel Ca current amplitude would be maximal at very short times and would then sag as depletion occurs. There are several reasons why this is not observed. First, at short distances where [Ca] may decline, the complementary error function in Eq. 2 will reach its steady-state level very rapidly (e.g., for $r = 3$ nm where the Ca_o depletion would be 2% in Fig. 3 *A*, the depletion would be 93% complete in 1 μs, see also Fig. 4 *A*). Even in the presence of binding (Fig. 4) the depletion at $r = 2$ nm is almost at the steady-state level in ~10 μs. This would be too fast to be detectable with the current bandwidth limitations of patch clamp systems. Second, for the depletions measured, the decrease in the electrochemical driving force for Ca through a channel would only be modest. At 2 mM $[Ca]_o$ a 40 μM depletion far from the channel (decreasing [Ca] to 1.96 mM) would have a negligible effect on the driving force for current flow. However, under conditions where large Ca_o depletions are predicted near the channel, the steady-state current is expected to decrease. Finally, single-channel Ca currents are usually measured at high Ca or Ba concentration and in a geometry which is closest to the semiinfinite model where depletions are small. At low [Ca] or [Ba] where larger depletions are expected, the current will be consequently reduced.

APPENDIX A

Writing the Laplacian in cylindrical coordinates, the boundary/initial-value problem of Eq. 7, is

$$\frac{D}{r}\frac{\partial}{\partial r}\left(r\frac{\partial c}{\partial r}\right) + D\frac{\partial^2 c}{\partial z^2} = \frac{\partial c}{\partial t}$$

$$D\frac{\partial c}{\partial z}(r, 0, t) = k\frac{\partial c}{\partial t}(r, 0, t) + \frac{q\delta(r)}{2\pi r}$$

$$c(r, z, 0) = c_0. \qquad \text{(A1)}$$

It is convenient to nondimensionalize Eq. A1 by making the change of variables

$$R = \frac{r}{k}, Z = \frac{z}{k}, T = \frac{Dt}{k^2}, C = \frac{2\pi kD}{q}(c - c_0), \qquad \text{(A2)}$$

which transforms Eq. A1 to

$$\frac{1}{R}\frac{\partial}{\partial R}\left(R\frac{\partial C}{\partial R}\right) + \frac{\partial^2 C}{\partial Z^2} = \frac{\partial C}{\partial T}$$

$$\frac{\partial C}{\partial Z}(R, 0, T) = \frac{\partial C}{\partial T}(R, 0, T) + \frac{\delta(R)}{R}$$

$$C(R, Z, 0) = 0, \qquad \text{(A3)}$$

where we have used the relation $\delta(kR) = \delta(R)/k$. We now solve the nondimensionalized problem A3 by taking its Laplace transform. Defining

$$\overline{C}(R, Z, s) = \mathcal{L}\{C(R, Z, T)\} = \int_0^\infty e^{-sT} C(R, Z, T)\, dT, \qquad \text{(A4)}$$

Eq. A3 becomes

$$\frac{1}{R}\frac{\partial}{\partial R}\left(R\frac{\partial \overline{C}}{\partial R}\right) + \frac{\partial^2 \overline{C}}{\partial Z^2} = s\overline{C} \qquad \text{(A5)}$$

$$\frac{\partial \overline{C}}{\partial Z}(R, 0, s) = s\overline{C}(R, 0, s) + \frac{\delta(R)}{Rs}. \qquad \text{(A6)}$$

Assuming a separable solution

$$\bar{C}(R, Z, s) = G(R, s)\, H(Z, s), \tag{A7}$$

and introducing the "separation constant" ζ^2 (independent of R and Z), Eq. A5 leads to

$$\frac{1}{RG}\frac{d}{dR}\left(R\frac{dG}{dR}\right) = s - \frac{1}{Z}\frac{d^2H}{dZ^2} = -\zeta^2, \tag{A8}$$

and therefore to

$$G(R, s)\, H(Z, s) = J_0(\zeta R)\exp\left(-(\zeta^2 + s)^{1/2}Z\right), \tag{A9}$$

where J_0 is the zero order Bessel function. $\bar{C}(R, Z, s)$ may be written as a superposition of solutions A9 for all possible values of ζ, $0 \le \zeta \le \infty$,

$$\bar{C}(R, Z, s) = \int_0^\infty A(\zeta, s)\, J_0(\zeta R)\exp\left(-(\zeta^2 + s)^{1/2}Z\right) d\zeta. \tag{A10}$$

$A(\zeta, s)$ is a function which is now determined by forcing Eq. A10 to satisfy the $Z = 0$ boundary condition of Eq. A6. Substituting Eq. A10 in Eq. A6 and setting $Z = 0$ yields

$$-\int_0^\infty A(\zeta, s)\left((\zeta^2 + s)^{1/2} + s\right) J_0(\zeta R)\, d\zeta = \frac{\delta(R)}{Rs}. \tag{A11}$$

An integral representation for the delta function in terms of a Bessel function that can be derived from the Fourier–Bessel integral (Morse and Feshbach, 1953) is

$$\delta(R) = R\int_0^\infty J_0(\zeta R)\zeta\, d\zeta. \tag{A12}$$

Substituting Eq. A12 for the right side of Eq. A11 and comparing the two sides of the equation, we obtain

$$A(\zeta, s) = \frac{-\zeta}{s\left((\zeta^2 + s)^{1/2} + s\right)}. \tag{A13}$$

Substituting this in Eq. A10 we have, finally

$$\bar{C}(R, Z, s) = -\frac{1}{s}\int_0^\infty J_0(\zeta R)\frac{\exp\left(-(\zeta^2 + s)^{1/2}Z\right)}{(\zeta^2 + s)^{1/2} + s}\zeta\, d\zeta. \tag{A14}$$

And $C(R, Z, t)$ is the inverse Laplace transform of Eq. A14.

Using the change of variables of Eq. A2 we can convert back to dimensional variables and obtain Eq. 8.

The integral in Eq. A14 was computed using a fourth-degree Newton-Cotes integration formula (Abramowitz and Stegun, 1964, formula 25.4.14) and an averaging technique which exploits the oscillatory behavior of J_0 to speed convergence of the integral (Dahlquist and Bjork, 1974). Without the averaging, the convergence problem is most severe for small values of Z. For $Z = 0$ (on the membrane surface), the integrand approaches zero as $\zeta^{-1/2}$ for large ζ. The integral is broken down into five segments, from zero to the sixth zero of $J_0'(x)$, where $x = (r/k)\zeta$ is the integration variable used in the computation, and four more segments between successive zeros of $J_0'(x)$ from the sixth ($x = 16.47\ldots$) through 10th zero ($x = 29.04\ldots$). The last four segments are given weighting factors of 15/16, 11/16, 5/16, and 1/16, respectively. This is equivalent to the procedure of repeated averaging of partial sums of an alternating series (Dahlquist and Bjork, 1974) and results in a rapid rate of convergence. The inverse Laplace transform is done using the numerical method of Stehfest (1970).

In the special case of $R = 0$ (i.e., along the channel axis), the argument of J_0 in Eq. A14 is zero, $J_0(0) = 1$, and there is no oscillation in the integrand. The above method does not apply in this case so that we handle it separately. Making the change of variables

$$\zeta = Z\left((\zeta + s)^{1/2} - s^{1/2}\right).$$

Eq. A14 for $R = 0$ becomes

$$\begin{aligned}\bar{C}(0, Z, s) &= -\frac{1}{s}\int_0^\infty \frac{\exp\left(-(\zeta^2 + s^{1/2}Z\right)}{(\zeta^2 + s)^{1/2} + s}\zeta\, d\zeta \\ &= -\frac{\exp\left(-s^{1/2}Z\right)}{sZ} \\ &\quad\cdot\int_0^\infty \frac{\exp(-\xi)\,(\xi + Zs^{1/2})}{\xi + Z(s + s^{1/2})}d\xi\end{aligned} \tag{A15}$$

which converges well because of the exp $(-\xi)$ term.

Equation A15 was used in Eq. 8 in place of Eq. A14 to compute the concentration along the channel axis (i.e., $c(r, z, t)$ at $r = 0$) in Fig. 4, *B* and *C*, whereas Eq. A14 was used to compute concentration on the membrane surface ($c(r, z, t)$ at $z = 0$) in Fig. 4, *A–C*.

APPENDIX B

To compute the contribution to the current from the surface-bound ions and from the bulk solution (Figs. 5 and 6), we need surface and volume integrals of Eq. 8. The number of moles of ions released from the surface between zero and r is

$$\begin{aligned}n_s(r, t) &= k\int_0^r [c_0 - c(r', 0, t)]2\pi r'\, dr' \\ &= \frac{q}{D}\mathcal{L}^{-1}\left\{\int_0^r\int_0^\infty \frac{J_0\left(\zeta\frac{r'}{k}\right)}{(\zeta^2 + s)^{1/2} + s}\zeta r'\, d\zeta\, dr'\right\} \\ &= \frac{qkr}{D}\mathcal{L}^{-1}\left\{\int_0^\infty \frac{J_1\left(\zeta\frac{r}{k}\right)}{(\zeta^2 + s)^{1/2} + s}d\zeta\right\} \\ &= \frac{qk^2}{D}\mathcal{L}^{-1}\left\{\int_0^\infty \frac{J_1(x)}{(x^2/R^2 + s)^{1/2} + s}dx\right\},\end{aligned} \tag{B1}$$

where we have used the known integral of J_0 (Abramowitz and Stegun, 1964) to obtain the third equality and made the transformation to $x = \zeta r/k = \zeta R$ for the numerical solution of Eq. B1. For large x, the integrand approaches zero as $x^{-3/2}$ (faster than in Eq. A14). For Eq. B1 the same procedure was used as for Eq. A14 except that because of the faster convergence the integral was taken only to the seventh zero J_1' at $x = 21.16\ldots$, with the 15/16, 11/16, 5/16, and 1/16 factors applied to the segments between the third and seventh zeroes.

The decrease in the number of moles in the hemispheric volume of radius r is

$$\begin{aligned} n_v(r,t) &= \int_0^r \int_0^{(r^2-z^2)^{1/2}} [c_0 - c(r',z',t)]2\pi r'\,dr'\,dz \\ &= \frac{q}{kD}\mathcal{L}^{-1}\left\{\frac{1}{s}\int_0^\infty \int_0^r \int_0^{(r^2-z^2)^{1/2}} J_0\left(\zeta\frac{r'}{k}\right) \right. \\ &\quad \left. \cdot \frac{\exp\left(-(\zeta^2+s)^{1/2}z/k\right)}{(\zeta^2+s)^{1/2}+s}\zeta r'\,dr'\,dz\,d\zeta \right. \\ &= \frac{q}{D}\mathcal{L}^{-1}\left\{\frac{1}{s}\int_0^\infty \int_0^r (r^2-z^2)^{1/2} J_1\left(\frac{\zeta(r^2-z^2)^{1/2}}{k}\right) \right. \\ &\quad \left. \cdot \frac{\exp\left(-(\zeta^2+s)^{1/2}z/k\right)}{(\zeta^2+s)^{1/2}+s}dz\,d\zeta \right. \\ &= \frac{qk^2}{D}\mathcal{L}^{-1}\left\{\frac{1}{s}\int_0^R \int_0^\infty J_1(x) \right. \\ &\quad \left. \cdot \frac{\exp\left(-(x^2/(R^2-Z^2)+s)^{1/2}Z\right)}{(x^2/(R^2-Z^2)+s)^{1/2}-s}dx\,dZ \right\}, \end{aligned} \tag{B2}$$

where we have made the transformation

$$x = \zeta(r^2-z^2)^{1/2}/k = \zeta(R^2-Z^2)^{1/2},$$

and reversed the order of integrations to obtain the last equality in B2. The same numerical procedure was used on the inner integral as was used in Eq. B1, but because of the second integration (over Z) in Eq. B2, the total computation time for Eq. B2 was considerably longer than for Eq. B1.

APPENDIX C

It is convenient to nondimensionalize the problem expressed by Eq. 15 and also to introduce a spatial variable measured from the center plane ($z = b$) rather than from the membrane ($z = 0$). The nondimensional variables

$$X = (b-z)/k,\ T = Dt/k^2,\ C = (c-c_0)D/kJ_z,\ B = b/k \tag{C1}$$

transform Eq. 15 to

$$\begin{aligned} \frac{\partial^2 C}{\partial X^2} &= \frac{\partial C}{\partial T} \\ \frac{\partial C}{\partial X}(0,T) &= 0 \\ -\frac{\partial C}{\partial X}(B,T) &= \frac{\partial C}{\partial T}(B,T) + 1 \\ C(X,0) &= 0. \end{aligned} \tag{C2}$$

If the Laplace transform is $\bar{C}(X,s) = \mathcal{L}C(X,T)$ then taking the Laplace transformation of Eqs. C2 yields

$$\begin{aligned} \frac{d^2\bar{C}}{dX^2} &= s\bar{C} \\ \frac{d\bar{C}}{dX}(0,s) &= 0 \\ -\frac{d\bar{C}}{dX}(B,s) &= s\bar{C}(B,s) + \frac{1}{s}. \end{aligned} \tag{C3}$$

The solution to the differential equation in C3 that satisfies the boundary condition at $X = 0$ is

$$\bar{C}(X,s) = A(s)\cosh(s^{1/2}X). \tag{C4}$$

Substituting C4 in the boundary condition at $X = B$ determines $A(s)$ to be

$$A(s) = 1/[s(s^{1/2}\sinh(s^{1/2}B) + s\cosh(s^{1/2}B))], \tag{C5}$$

and the nondimensional concentration is

$$C(X,T) = \mathcal{L}^{-1}\left\{\frac{-\cosh(s^{1/2}X)}{s(s^{1/2}\sinh(s^{1/2}B) + s\cosh(s^{1/2}B))}\right\} \tag{C6}$$

Transforming back to dimensional variables yields Eq. 16.

Using the Taylor series expansions of the hyperbolic sine and cosines yields

$$\begin{aligned} C(X,T) &= \mathcal{L}^{-1}\left\{\frac{-1 - \frac{s}{2}\left(X^2 - \frac{B^2(B+3)}{3(B+1)}\right) + O(s^2)}{s^2(B+1)}\right\} \\ &= \frac{-1}{B+1}\left(T + \frac{X^2}{2} - \frac{B^2(B+3)}{6(B+1)} + O(T^{-1})\right), \end{aligned} \tag{C7}$$

transforming to dimensional variables yields Eq. 17.

APPENDIX D

Eq. 19 and the associated initial and boundary conditions are

$$\begin{aligned} D\partial^2 c/\partial x^2 - \partial c/\partial t &= Q \\ c(0,t) &= c_0 \\ \partial c/\partial x(\ell,t) &= 0 \\ c(x,0) &= c_0. \end{aligned} \tag{D1}$$

Making the transformation

$$u(x,t) = c(x,t) - c_0 - Qx(\ell - x/2)/D, \tag{D2}$$

i.e., subtracting $c(x,\infty)$ from $c(x,t)$, converts D1 to the homogenous problem

$$\begin{aligned} D\partial^2 u/\partial x^2 - \partial u/\partial t &= 0 \\ u(0,t) &= 0 \\ \partial u/\partial x(\ell,t) &= 0 \\ u(x,0) &= Qx(\ell - x/2)/D, \end{aligned} \tag{D3}$$

which may be solved in the form of an eigenfunction expansion. Assuming a separable solution for D3 of the form $u(x, t) = F(x)\,G(t)$, we find that $F(x) = \sin[(n + \frac{1}{2})\pi x/\ell]$ and $G(t) = \exp[-(n + \frac{1}{2})^2\pi^2 Dt/\ell^2]$ satisfy the equation and two boundary conditions, where n is an integer. The solution to D3 thus may be written as an infinite sum

$$u(x, t) = \sum_{n=0}^{\infty} A_n \sin[(n + \tfrac{1}{2})\pi x/\ell] \cdot \exp[-(n + \tfrac{1}{2})^2\pi^2 Dt/\ell^2], \quad \text{(D4)}$$

where A_n is determined by requiring D4 to satisfy the initial condition in D3,

$$\sum_{n=0}^{\infty} A_n \sin[(n + \tfrac{1}{2})\pi x/\ell] = Qx(\ell - x/2)/D. \quad \text{(D5)}$$

Multiplying both sides of Eq. D5 by $\sin[(m + \frac{1}{2})\pi x/\ell]$ and integrating from $x = 0$ to $x = \ell$, using the orthogonality of the sine functions to evaluate the left side and tabulated integrals to evaluate the right side, we obtain

$$A_m \ell/2 = Q\ell^3/[(m + \tfrac{1}{2})^3\pi^3 D], \quad \text{(D6)}$$

and using the result D6 in D4, yields the solution to D3

$$u(x, t) = \frac{2\ell^2 Q}{\pi^3 D} \sum_{n=0}^{\infty} \frac{\sin[(n + \frac{1}{2})\pi x/\ell]}{(n + \frac{1}{2})^3} \cdot \exp(-(n + \tfrac{1}{2})^2\pi^2 Dt/\ell^2). \quad \text{(D7)}$$

This solution can also be obtained by transforming the solution to a related heat conduction problem in a slab with heat produced within it (Carslaw and Jaeger, 1959, formula 3.14 [7]). Substituting Eq. D7 for $u(x, t)$ in Eq. D2 yields Eq. 22. Fig. 10 *B* shows $c(x, t)$ as a function of x for several values of t. Eq. 22 is valid as long as the monotonically decreasing curves remain positive for $0 \le x < \ell$. This is not true for t somewhat >50 ms for the case illustrated, i.e., the Ca current is sufficient to cause total depletion of Ca somewhere before the end to the tubule. In this case the appropriate boundary/initial value problem is

$$D\partial^2 c/\partial x^2 - \partial c/\partial t = Q$$
$$c(0, t) = c_0$$
$$c(b, t) = 0 = \partial c/\partial x(b, t)$$
$$c(x, 0) = c_0, \quad \text{(D8)}$$

where $x = b \le \ell$ is the location where the concentration and the flux both must be zero. From Eq. 22, we know the solution for the flux vanishing at $x = b$ (just replace ℓ by b in Eq. 22). In addition, we now must also require that c vanish at $x = b$ which leads to the equation

$$c_0 = \frac{Qb^2}{2D} \cdot \left\{1 - \frac{4}{\pi^3} \sum_{n=0}^{\infty} \frac{(-1)^n}{(n + \frac{1}{2})^3} \exp(-(n + \tfrac{1}{2})^2\pi^2 Dt/b^2)\right\} \quad \text{(D9)}$$

which can be solved numerically for b.

Substituting Eq. D9 in Eq. 22 with $\ell = b$ we obtain

$$c(x, t) = \frac{Q}{2D}(b - x)^2 + \frac{2b^2 Q}{\pi^3 D} \sum_{n=0}^{\infty} \frac{\sin[(n + \frac{1}{2})\pi x/b] - (-1)^n}{(n + \frac{1}{2})^3} \cdot \exp(-(n + \tfrac{1}{2})^2\pi^2 Dt/b^2). \quad \text{(D10)}$$

In the special case of $t = \infty$, all terms in the summations in Eqs. D9 and D10 vanish and the result reduces to Eq. 23.

We thank Dr. Eli Engel for comments on an earlier version of this manuscript.

This work was supported in part by a grant from the National Institutes of Health (NIH, HL30077). Donald M. Bers is the recipient of a Research Career Development Award from the NIH (HL01526).

Received for publication 21 May 1990 and in final form 2 November 1990.

REFERENCES

Abramowitz, M., and I. A. Stegun, editors. 1964. Handbook of Mathematical Functions. NBS Applied Mathematics Series 55.

Almers, W., R. Fink, and P. T. Palade. 1981. Calcium depletion in frog muscle tubules: the decline of calcium current under maintained depolarization. *J. Physiol. (Lond.).* 312:177–207.

Andersen, O. S. 1983. Ion movement through gramicidin A channels. Interfacial polarization effects on single-channel current measurements. *Biophys. J.* 41:135–146.

Bean, B. P., M. C. Nowycky, and R. W. Tsien. 1984. β-Adrenergic modulation of calcium channels in frog ventricular heart cells. *Nature (Lond.).* 307:371–375.

Bers, D. M. 1983. Early transient depletion of extracellular [Ca] during individual cardiac muscle contractions. *Am. J. Physiol.* 244:H462–H468.

Bers, D. M. 1985. Ca influx and SR Ca release in cardiac muscle activation during postrest recovery. *Am. J. Physiol.* 248:H366–H381.

Bers, D. M. 1987. Mechanisms contributing to the cardiac inotropic effect of Na-pump inhibition and reduction of extracellular Na. *J. Gen. Physiol.* 90:479–504.

Bers, D. M., and G. A. Langer. 1979. Uncoupling cation effects on cardiac contractility and sarcolemmal Ca^{2+} binding. *Am. J. Physiol.* 237:H332–H341.

Bers, D. M., K. D. Philipson, and G. A. Langer. 1981. Cardiac contractility and sarcolemmal calcium binding in several cardiac preparations. *Am. J. Physiol.* 240:H576–H583.

Bers, D. M., K. D. Philipson, and A. Peskoff. 1985. Calcium at the surface of cardiac plasma membrane vesicles:cation binding, surface charge screening and Na-Ca exchange. *J. Membr. Biol.* 85:251–261.

Bers, D. M., L. A. Allen, and Y. Kim. 1986. Calcium binding to cardiac sarcolemma isolated from rabbit ventricular muscle: its possible role in modifying contractile force. *Am. J. Physiol.* 251:C861–C871.

Brum, G., W. Osterrieder, and W. Trautwein. 1984. β-Adrenergic increase in the calcium conductance of cardiac myocytes studies with the patch-clamp. *Pfluegers Arch. Eur. J. Physiol.* 401:111–118.

Cachelin, A. B., J. E. DePeyer, S. Kokubun, and H. Reuter. 1983. Ca^{2+} channel modulation by 8-bromocyclic AMP in cultured heart cells. *Nature (Lond.).* 304:462–464.

Carslaw, H. S., and J. C. Jaeger. 1959. Conduction of Heat in Solids. 2nd ed. Oxford University Press, Briston, England.

Cleeman, L., G. Pizarro, and M. Morad. 1984. Optical measurements of extracellular calcium depletion during a single heartbeat. *Science (Wash. DC).* 226:174–177.

Coronado, R., and H. Affolter. 1986. Insulation of the conduction pathway of muscle transverse tubule calcium channels from the surface charge of bilayer phospholipid. *J. Gen. Physiol.* 87:933–953.

Crank, J. 1975. The Mathematics of Diffusion. 2nd ed. Oxford University Press, Briston, England. 414 pp.

Dahlquist, G., and A. Bjork. 1974. Numerical Methods. Prentice-Hall, Englewood Cliffs, NJ. Sec. 3.2.1. 573 pp.

Dresdner, K. P., and R. P. Kline. 1985. Extracellular calcium ion depletion in frog cardiac ventricular muscle. *Biophys. J.* 48:33–45.

Eigen, M., and L. De Maeyer. Relaxation methods. 1963. *In* Technique of Organic Chemistry. Vol. VIII. S. L. Friess, E. S. Lewis, and A. Weissberger, editors. Interscience Publishers, Division John Wiley & Sons Ltd., New York. 895–1124.

Fenwick, E. M., A. Marty, and E. Neher. 1982. Sodium and calcium channels in bovine chromaffin cells. *J. Physiol. (Lond.).* 331:599–635.

Fischmeister, R., and M. Horackova. 1983. Variation of intracellular Ca^{2+} following Ca^{2+} current in heart. *Biophys. J.* 41:341–348.

Frank, J. S., and G. A. Langer. 1974. The myocardial interstitium: its structure and its role in ionic exchange. *J. Cell Biol.* 60:586–601.

Hainsworth, A. H., and S. B. Hladky. 1987. Effects of double-layer polarization on ion transport. *Biophys. J.* 51:27–36.

Hess, P., J. B. Lansman, and R. W. Tsien. 1984. Different modes of Ca channel gating behavior favored by dihydropyridine Ca agonists and antagonists. *Nature (Lond.).* 311:538–544.

Hilgemann, D. W. 1986. Extracellular calcium transients at single excitations in rabbit atrium measured with tetramethylmurexide. *J. Gen. Physiol.* 87:707–735.

Hodgkin, A. L., and R. D. Keynes. 1957. Movements of labelled calcium in squid giant axons. *J. Physiol. (Lond.).* 138:253–281.

Kushmerick, M. J., and R. J. Podolsky. 1969. Ionic mobility in muscle cells. *Science (Wash. DC).* 166:1297–1298.

Langer, G. A., J. S. Frank, and K. D. Philipson. 1982. Ultrastructure and calcium exchange of the sarcolemma, sarcoplasmic reticulum and mitochondria of the myocardium. *Pharmacol. Ther.* 16:331–376.

London, B., and J. W. Krueger. 1986. Contraction in voltage-clamped, internally perfused single heart cells. *J. Gen. Physiol.* 88:475–505.

McCleskey, E. W., and W. Almers. 1985. The Ca channel in skeletal muscle is a large pore. *Proc. Natl. Acad. Sci. USA.* 82:7149–7153.

McDonald, T. F., H. Nawarth, and W. Trautwein. 1975. Membrane currents and tension in cat ventricular muscle treated with cardiac glycosides. *Circ. Res.* 37:674–682.

McDonald, T. F., A. Cavalie, W. Trautwein, and D. Pelzer. 1986. Voltage-dependent properties of macroscopic and elementary calcium channel currents in guinea pig ventricular myocytes. *Pfluegers Arch. Eur. J. Physiol.* 406:437–448.

Morse, P. M., and H. Feshback. 1953. Methods of Theoretical Physics. McGraw-Hill Inc., New York. 1978 pp.

Nasi, E., and D. Tillotson. 1985. The rate of diffusion of Ca^{2+} and Ba^{2+} on a nerve cell body. *Biophys. J.* 47:735–738.

Niedergerke, R. 1957. The rate of action of calcium ions on the contraction of the heart. *J. Physiol. (Lond.).* 138:506–515.

Page, E., L. P. McCallister, and B. Power. 1971. Stereological measurements of cardiac ultrastructures implicated in excitation-contraction coupling. *Proc. Natl. Acad. Sci. USA.* 68:1465–1466.

Page, E. 1978. Quantitative ultrastructural analysis in cardiac membrane physiology. *Am. J. Physiol.* 235:C147–C158.

Peskoff, A., and D. M. Bers. 1987. Electrodiffusion of ions converging toward the mouth of a channel. *Biophys. J.* 51:395a. (Abstr.)

Peskoff, A., and D. M. Bers. 1988. Electrodiffusion of ions approaching the mouth of a conducting membrane channel. *Biophys. J.* 53:863–875.

Philipson, K. D., D. M. Bers, and A. Y. Nishimoto. 1980*a*. The role of phospholipids in Ca^{2+} binding of isolated cardiac sarcolemma. *J. Mol. Cell. Cardiol.* 12:1159–1173.

Philipson, K. D., D. M. Bers, A. Y. Nishimoto, and G. A. Langer. 1980*b*. The binding of calcium and sodium to sarcolemmal membranes: relation to the control of myocardial contractility. *Am. J. Physiol.* 238:H373–H378.

Post, J. A., G. A. Langer, J. A. F. Op den Kamp, and A. J. Verkleij. 1988. Phospholipid asymmetry in cardiac sarcolemma. Analysis of intact cells and "gas-dissected" membranes. *Biochim. Biophys. Acta.* 943:256–266.

Safford, R. E., and J. B. Bassingthwaighte. 1977. Calcium diffusion in transient and steady states in muscle. *Biophys. J.* 20:113–136.

Shattock, M. J., and D. M. Bers. 1989. Rat vs. rabbit ventricle: Ca flux and intracellular Na assessed by ion-selective microelectrodes. *Am. J. Physiol.* 256:C813–C822.

Sommer, J. R., and R. B. Jennings. 1986. Ultrastructure of cardiac muscle. *In* The Heart and Cardiovascular System. H. A. Fozzard, E. Haber, R. B. Jennings, A. M. Katz, and H. E. Morgan, editors. Raven Press Ltd., New York. 61–100.

Stehfest, H. 1970. Numerical inversion of Laplace transforms. *Commun. Assoc. Comput. Machinery.* 13:47–49.

Tsien, R. W., B. P. Bean, P. Hess, and M. C. Nowycky. 1983. Calcium channels: mechanisms of β-adrenergic modulation and ion permeation. *Cold Spring Harbor Symp. Quant. Biol.* 47:201–212.

Wang, J. H. 1953. Tracer-diffusion in liquids. IV. Self-diffusion of calcium ion and chloride ion in aqueous calcium chloride solutions. *J. Am. Chem. Soc.* 75:1769–1770.

Yue, D. T., and E. Marban. 1990. Permeation in the dihydropyridine-sensitive calcium channel. *J. Gen. Physiol.* 95:911–939.

Zwaal, R. F. A., B. Roelofsen, and C. M. Colley. 1973. Localization of red cell membrane constituents. *Biochim. Biophys. Acta.* 300:159–182.